DOI 10.1007/s11182-020-01950-7

Russian Physics Journal, Vol. 62, No. 11, March, 2020 (Russian Original No. 11, November, 2019)

MICROARC OXIDATION OF METAL SURFACES: COATING PROPERTIES AND APPLICATIONS

S. S. Arbuzova,[1] P. I. Butyagin,[1] A. V. Bol'shanin,[1] A. I. Kondratenko,[1] and A. V. Vorob'ev[2]

UDC 544.653

The paper deals with one of the most promising, intensively developing methods of depositing functional oxide coatings onto aluminum and titanium alloys, namely microarc oxidation (MAO) performed in the pulsed current mode. MAO layers can be obtained due to both oxidation of the substrate material and thermochemical transformations of electrolyte components and their subsequent melting on the part surface. It is shown how the black coating appears on the surface of aluminum and titanium alloys due to the MAO process. The structure, phase and elemental compositions of the resulting coatings are studied in this paper.

Keywords: microarc oxidation, coating, aluminum and titanium alloys.

INTRODUCTION

Currently, microarc oxidation in electrolytic solutions using pulsed power supply is being widely used in industries. This method allows forming nanostructured nonmetallic inorganic coatings on the surface of aluminum, titanium, zirconium, magnesium and their alloys [1–3]. The properties of such coatings depend on such factors as microarc oxidation (MAO) modes, the electrolyte nature, the alloy composition and the specimen geometry. A lot of the MAO systems that provide metal-surface coatings with high hardness, wear and corrosion resistances, dielectric strength are known [2].

The essence of the MAO technique is that when the high-density current passes through the metal/electrolyte interface, the voltage at this interface becomes higher than its dielectric strength, and microarc discharges with high local temperatures and pressures occur on the electrode surface. The resulting coating layer consists of oxidized elements of the substrate material and the electrolyte elements [3, 4].

In works [2, 5] it was shown that the following processes occurred in electrolytic solution during microarc discharges:

1. Electrochemical reactions of ion discharge on the surface.
2. Delivery of ions from the solution to the surface.
3. Barrier breakdown phenomenon with the formation of microarc discharges.
4. High-temperature chemical and electrochemical reactions.

All these processes are interconnected and run consistently. Understanding of the microarc oxidation process allows controlling the formation and the quality of the obtained coating with certain functional properties.

The microarc oxidation system developed at AO MANEL (Tomsk, Russia) provides the coating synthesis of white, black, brown, green colors and their various tones. Recently, black coating has become a matter of increasing interest from customers due to its optical properties.

[1]AO MANEL, Tomsk, Russia, e-mail: svetlana.safronova@manel.ru; pavel.butyagin@manel.ru; anton.bolshanin@manel.ru; anton.kondratenko@elesy.ru; [2]National Research Tomsk Polytechnic University, Tomsk, Russia, e-mail: bonsoirmonami@mail.ru. Translated from Izvestiya Vysshikh Uchebnykh Zavedenii, Fizika, No. 11, pp. 117–122, November, 2019. Original article submitted September 13, 2019.

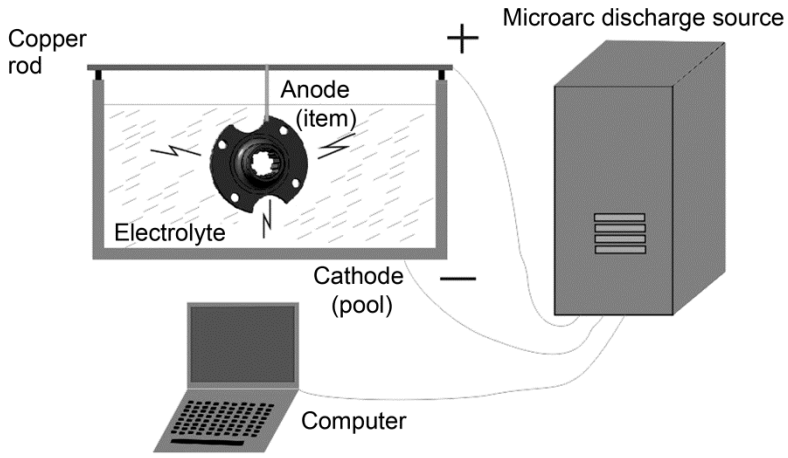

Fig. 1. Schematic of the microarc oxidation system from AO MANEL, Tomsk, Russia.

The purpose of this work is to investigate the phase composition, morphology and microstructure of the black coating deposited onto the surface of aluminum and titanium alloys and synthesized by microarc oxidation in the weak-acid "Manel-Black" electrolyte.

MATERIALS AND METHODS

Grades D16T (AISI 2024, USA) and AMg2 (ASTM B221, USA) aluminum alloys and VT1-0 (ASTM Grade 2, USA) titanium alloy were used in this experiment. All the specimens were cleaned and degreased before the MAO process.

Schematic of the microarc oxidation system manufactured at AO MANEL is illustrated in Fig. 1. The coating deposition was performed by using an ARCCOR switch-mode power supply produced by AO EleSi, Tomsk, Russia. The process parameters included 600 V voltage, 50 Hz frequency, 200 μs pulse time, and weak-acid "Manel-Black" electrolyte (pH = 6). After treatment, the specimens were dried at 100°C in a drying box.

The average rate of the ceramic-like coating deposition onto the anode was 1 μm/min, which was more intensive at the beginning and lowered with decreasing thickness of the oxide layer. In [6], such a difference in the deposition rate was explained by active current dependent on the substances involved in the electrochemical reaction.

The microstructure and elemental composition of the coating were studied on a dual-beam scanning electron microscope (SEM) Quanta 200 3D (Netherlands). An Agilent G200 Nanoindenter fitted with a Berkovich three-sided diamond pyramid tip with a rounding of 20 nm was used for nanoindentation examinations. X-ray diffraction patterns (XRD) of composites were obtained using a Shimadzu XRD-6000 diffractometer (Japan). Measurements were conducted using copper radiation (K_α). An Ascott CC450iP cyclic corrosion test chamber (Great Britain) was used to perform cyclic corrosion tests at (35±2) °C for 1500 hours. Tests were carried out in conformity with the Russian state standard. The coating thickness was measured by a QuaNix 7500 coating thickness gauge (Germany).

RESULTS AND DISCUSSION

During the MAO process, a transition layer 5–20 μm thick appearing at the metal/coating interface strengthens the adhesion between them and restricts the access of the aggressive substance to the metal/coating interface. The thickness of the outer layer ranges between 20 and 40 μm.

The results of the elemental analysis gathered in Table 1 show that in the MAO process, the substrate material discharges into the solution and then precipitates onto the surface. The Al content in the coating on the Al substrate

TABLE 1. Elemental Composition of Protective Black Coating of Different Thickness on Al and Ti Alloys

Alloy grades	Coating thickness, μm	Content, %								
		O	Na	Al	Si	P	Mo	K	Fe	Ti
AISI 2024 Al alloy	20	17.46	0.97	11.16	0.16	18.94	3.12	1.28	46.90	–
	35	17.25	1.11	16.06	0.13	15.76	2.35	0.96	46.38	–
	55	17.55	0.93	19.71	–	13.48	1.63	0.82	45.88	–
ASTM B221 Al alloy	20	17.68	0.67	11.01	0.20	19.56	3.25	1.05	46.59	–
	35	17.45	1.07	16.08	0.14	16.08	2.55	1.03	45.60	–
	55	17.61	0.84	20.08	–	13.88	1.79	0.79	45.00	–
ASTM Grade 2 Ti	20	21.03	1.14	–	–	21.39	4.01	1.49	32.11	18.83
	35	19.68	0.98	–		19.58	2.87	1.25	32.22	22.78
	55	20.82	1.15	–		18.83	3.81	1.44	29.93	24.03

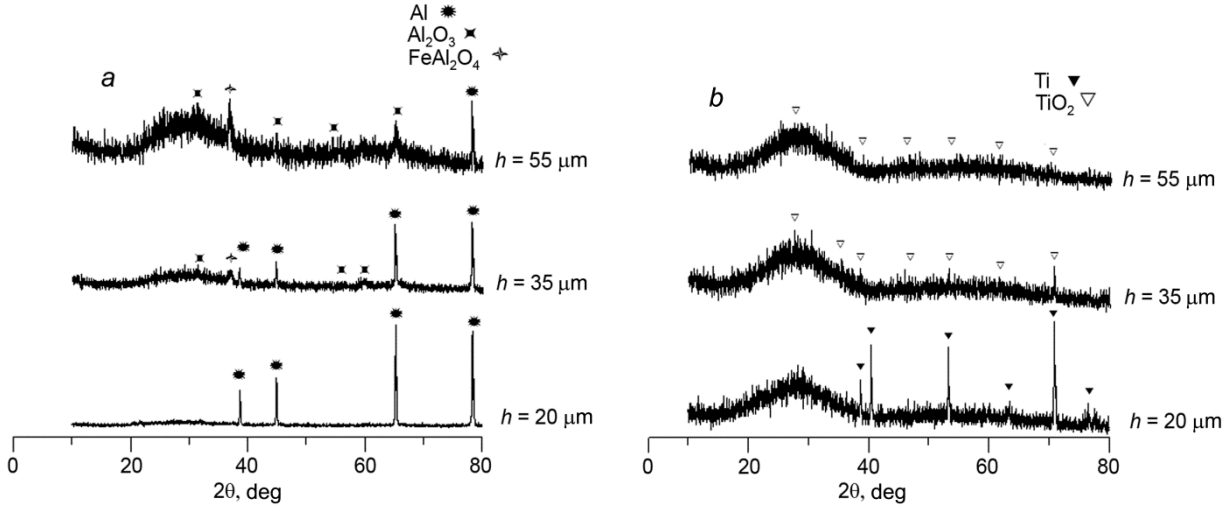

Fig. 2. XRD patterns of the MAO coating on the AISI 2024 Al (*a*) and ASTM Grade 2 Ti (*b*) alloys.

varies from 10 to 20%, whereas the Ti content in the coating on the Ti substrate varies from 18 to 24%. With increasing coating thickness, the Al and Ti content on the coating surface increases. The most probable components, which also increase the microarc thickness, are electrolyte elements (P, Mo, Fe), which adsorb and partly embed into the coating structure with the formation of various compounds. In addition to the electrolyte elements, the detected iron content in the coating is higher than that of aluminum and titanium. The XRD analysis of the aluminum alloys shows the formation of $FeAl_2O_4$ (spinel) phase, which provides dull black color to the coating.

According to Fig. 2 presenting the XRD patterns for the phase composition of the MAO coating on the titanium alloy (ASTM Grade 2), the Ti substrate reflections are observed at the coating thickness of 20 μm. With increasing coating thickness, the formation of the TiO_2 rutile phase occurs due to the microarc discharge at a voltage of over 450 V. The diffused reflection indicates to the presence of the X-ray amorphous phase. The black color of the coating on the Ti substrate can be provided by the formation of the $FeTiO_3$ phase, which is black in nature and forms similarly to the spinel phase on the Al substrates.

Mikheev, *et al*. [7] demonstrated that along with $FeAl_2O_4$ and $FeTiO_3$ spinel phases, the formation of K_3FeO_4 and Fe_2O_3 phases occurs during microarc oxidation of Al and Ti alloys in electrolytic solutions containing potassium ferricyanide.

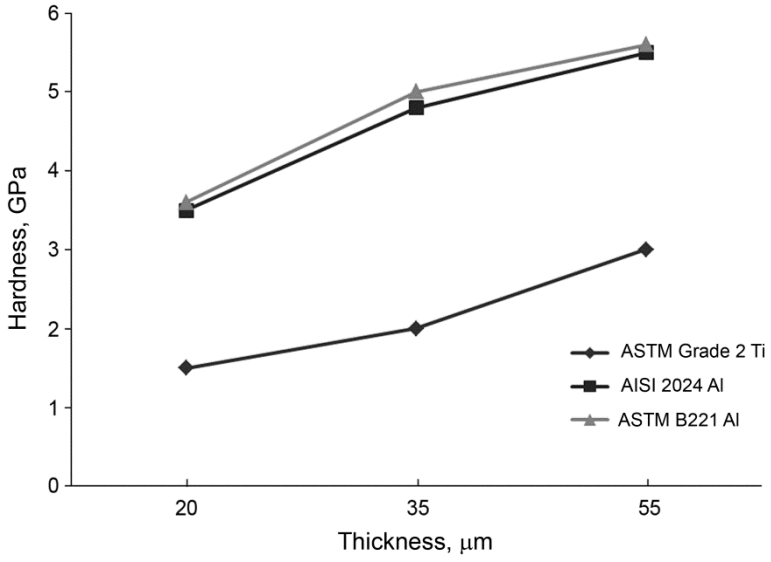

Fig. 3. Coating hardness/thickness dependence.

The indentation technique was used to determine the mechanical characteristics of these coatings. At the indentation load of 100 mN, the depth of indentation did not exceed 10% of the coating thickness, which allowed us to determine the mechanical properties of the coating without the substrate influence.

As can be seen from Fig. 3 presenting the coating hardness/thickness dependence, the hardness increases with the thickness growth. The AISI 2024 and ASTM B221 Al alloys have the highest microhardness of the MAO coating, *i.e.* 5.6 and 5.8 GPa, respectively, at 55 μm thickness.

The hardness of the MAO coating on the ASTM Grade 2 is 2.8 GPa, which is almost 2 times lower than on aluminum specimens. According to the Mohs scale of mineral hardness, the hardness of Al-based compounds is higher than that of Ti-based, *viz*. 8 and 5, respectively. Lavrushin, *et al.* [8] report that the X-ray amorphous phase presenting in the coating composition on titanium specimens is more plastic than the crystalline phase, and promotes relaxation of mechanical stresses arising during deformation. It can therefore be assumed that X-ray amorphous titanium dioxide in the black coating on the titanium substrate and modified by aluminum, iron, phosphorus and molybdenum compounds, allows us to synthesize a more plastic coating (49% degree of crystallinity) as compared to that on the aluminum substrate, where the crystalline phase ranges from 60 to 80%.

One of the key problems of non-failure operation is corrosion protection. Corrosion protection of the substrate material can be provided by the coating thickness and control for the pore amount and morphology. A study of morphology of the MAO coating synthesized in the weak-acid “Manel-Black” electrolyte on the Al and Ti substrates using the above indicated modes, shows that the pore size varies from 2 to 5 μm at the coating thickness of 20 μm. As shown in Fig. 4, the coating morphology changes with increasing thickness: the total amount of pores decreases, and larger (10–15 μm) pores appear. These changes in the coating morphology are observed for all the investigated specimens regardless of the substrate material. Thus, changing the time of the microarc oxidation process it is possible to produce coatings of the required thickness and porosity.

Table 2 gives the values of the coating thickness for different alloys and their corrosion resistance, which was tested in the cyclic corrosion test chamber at (35±2)°C during 1500 hours in conformity with the Russian state standard. Corrosion damages were detected visually by changes in the color and the corrosion spot size.

According to Table 2, the corrosion resistance grows with increasing coating thickness. All tests demonstrate the high corrosion resistance for the coatings on both the ASTM B221 Al and ASTM Grade 2 Ti. The MAO coatings deposited onto the AISI 2024 Al with reduced corrosion resistance provide its increased service life. After 460-hour tests for coatings synthesized in the cyclic corrosion chamber, only the first evidence of corrosion appear on the AISI 2024 Al in the form of individual dark spots 0.1–0.5 mm in size. The degree of the surface corrosion of this specimen

TABLE 2. Results of Corrosion Resistance Testing

Alloy grades	Coating thickness, μm	Surface corrosion, %						
		0–24 h	96 h	294 h	460 h	720 h	1000 h	1500 h
AISI 2024	20	0			2	10	20	30
	35	0			1	5	10	15
	55	0				1	5	7
ASTM B221	20	0						1
	35	0						1
	55	0						1
ASTM Grade 2	20	0						
	35	0						
	55	0						

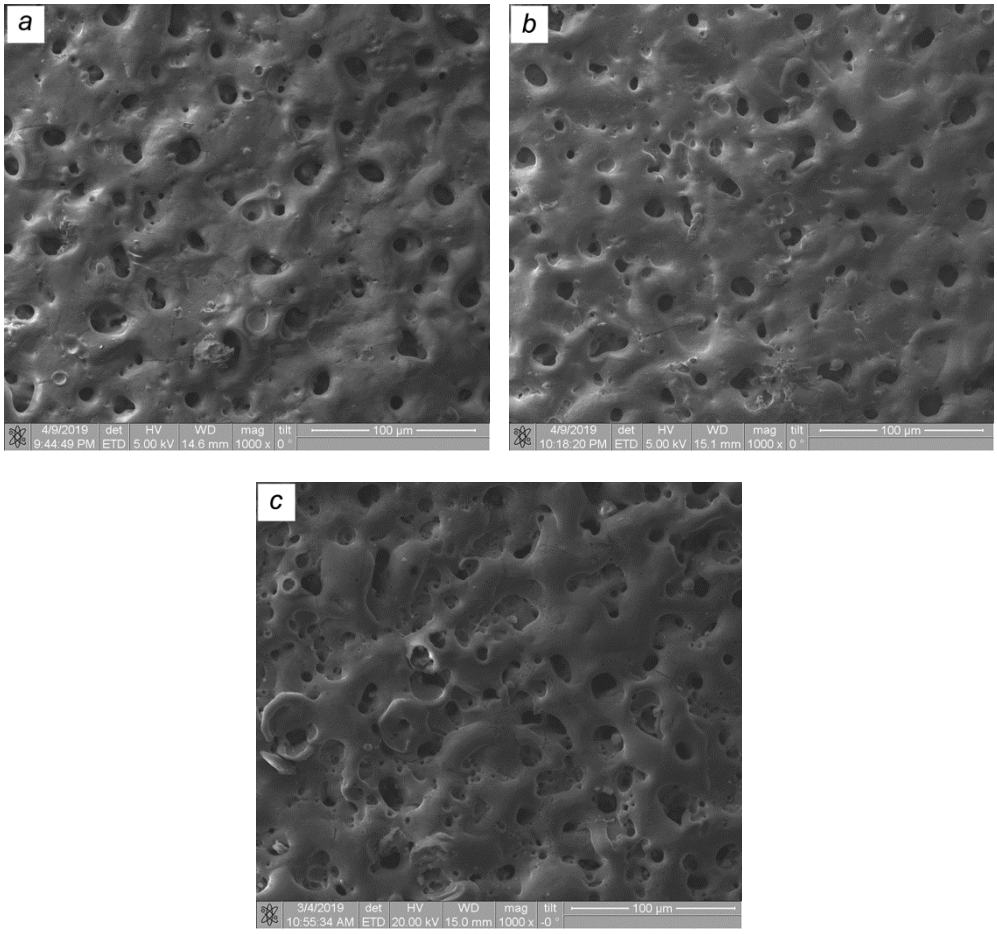

Fig. 4. SEM images of the specimen surface with the MAO coating 55 μm thick: *a* – AISI 2024 Al, *b* – ASTM B221 Al, *c* – ASTM Grade 2 Ti.

ranges between 0 and 2%. With further increase in the testing time up to 1500 h, the specimens with the coating thickness of 35–55 μm manifest the best protective properties. Thus, the corrosion tests confirm the literature data on the substrate material importance in the coating corrosion resistance.

CONCLUSIONS

Based on the results, in can be concluded that the MAO coating contained the elements of both the substrate material (Al, Ti) and the electrolyte (P, Fe, Mo), which proved the mechanism of the coating formation proposed in [2, 5]. The formation of $FeAl_2O_4$ and $FeTiO_3$ phases blackened the coating obtained. Unlike the Al alloys, the Grade 2 Ti alloy demonstrated the formation of the X-ray amorphous phase at different thickness of the Grade 2 Ti alloy which had the lowest hardness of 2.8 GPa among the specimens at issue. The same tendency was observed in forming the porous morphology of the coating, namely: with increasing coating thickness, the total amount of pores reduced and their size grew. Despite this, the corrosion resistance of the specimens differed due to the nature of the alloy. The highest corrosion resistance was observed in coatings on the Grade 2 Ti and the ASTM B221 Al. The coating deposition onto the AISI 2024 Al substrates having the reduced corrosion resistance improved their service life also.

REFERENCES

1. V. N. Borikov, Methods and means of measuring electrical parameters of pulsed energy coating deposition in solutions, Author's Abstract Doc. Sci. Dissert., TPU, Tomsk (2011).
2. A. I. Mamaev and V. A. Mamaeva, High-Current Microarc Processes in Electrolyte Solutions [in Russian], RAS Siberian Division, Novosibirsk (2005).
3. E. V. Khokhryakov, Physical and chemical regularities of formation of multi-component functional coatings in microplasma mode, Author's Abstract Cand. Chem. Sci. Dissert., TSU, Tomsk (2004).
4. P. I. Butyagin, E. V. Khokhryakov, and A. I. Mamaev, Gal'vanotekhnika i obrabotka poverkhnosti, No. 2, 21–23 (2003).
5. A. I. Mamaev, V. A. Mamaeva, E. Yu. Beletskaya, *et al*., Russ. Phys. J., **56**, No. 8, 959–969 (2013).
6. T. I. Dorofeeva, Yu. Yu. Budnitskaya, A. K. Chubenko, *et al*., Izv. Vyssh. Uchebn. Zaved., Fiz., **54**, No. 9/2, 108–113 (2011).
7. A. E. Mikheev, A. V. Girn, D. V. Orlova, *et al*., Vestnik SIBSAU, **44**, No. 4, 168–172 (2012).
8. G. A. Lavrushin, S. V. Gnedenkov, P. S. Gordienko, *et al*., Prot. Met., **38**, No. 4, 363-365 (2002).